J. Fluid Mech. (2011), *vol.* 688, *pp.* 528–550.
doi:10.1017/jfm.2011.400

Numerical computation of solitary waves in a two-layer fluid

H. C. Woolfenden† and E. I. Părău

School of Mathematics, University of East Anglia, Norwich NR4 7TJ, UK

(Received 27 April 2011; revised 19 July 2011; accepted 15 September 2011;
first published online 7 November 2011)

We consider steady two-dimensional flow in a two-layer fluid under the effects of gravity and surface tension. The upper fluid is bounded above by a free surface and the lower fluid is bounded below by a rigid bottom. We assume the fluids to be inviscid and the flow to be irrotational in each layer. Solitary wave solutions are found to the fully nonlinear problem using a boundary integral method based on the Cauchy integral formula. The behaviour of the solitary waves on the interface and free surface is determined by the density ratio of the two fluids, the fluid depth ratio, the Froude number and the Bond numbers. The dispersion relation obtained for the linearized equations demonstrates the presence of two modes: a 'slow' mode and a 'fast' mode. When a sufficiently strong surface tension is present only on the free surface, there is a region, or 'gap', between the two modes where no linear periodic waves are found. In-phase and out-of-phase solitary waves are computed in this spectral gap. Damped oscillations appear in the tails of the solitary waves when the value of the free-surface Bond number is either sufficiently small or large. The out-of-phase waves broaden as the Froude number tends towards a critical value. When surface tension is present on both surfaces, out-of-phase solitary waves are computed. Damped oscillations occur in the tails of the waves when the interfacial Bond number is sufficiently small. Oppositely oriented solitary waves are shown to coexist for identical parameter values.

Key words: capillary waves, solitary waves

1. Introduction

This study is concerned with solitary waves propagating in two-fluid systems with free-surface boundary conditions. Examples are the interfacial waves that occur at the sharp interface between two layers of water of different densities due to, for example, the variation in salinity and temperature (e.g. Phillips 1966; Baines 1995). They have an important effect on submerged constructions such as oil platforms and pipes lying on the seabed (Osborne, Burch & Scarlet 1978). Interfacial waves can also be easily observed experimentally (e.g. Michallet & Barthelemy 1998; Mercier, Vasseur & Dauxois 2011). There is also a mathematical interest in the study of various nonlinear evolution equations that occur in the theory of interfacial waves.

The influence of interfacial or internal waves on oceanic surface waves has been a subject of oceanographic interest for several decades. There are many observations of the so-called 'dead-water' effect, first reported by Ekman (1904). He described

† Email address for correspondence: h.woolfenden@uea.ac.uk

a strange phenomenon observed in 1893, when the ship of the Norwegian explorer F. Nansen met a strong resistance on the Barents Sea, with no waves visible at the surface and no wind. Very recently, Mercier *et al.* (2011) reproduced the 'dead-water' effect in laboratory experiments. They observed that large-amplitude nonlinear interfacial waves were generated by a moving object, while no waves were visible on the free surface. The surface and interfacial tensions play a pivotal role on the wave generation in the experiments owing to the small depths involved. Therefore it is of paramount importance to understand and quantify the effect that the tensions make to the governing dynamics.

There has been important progress in studying nonlinear interfacial waves in the last 20 years – see Helfrich & Melville (2006) for a review of steady internal solitary waves. Choi & Camassa (1996, 1999) have derived weakly and fully nonlinear model equations for interfacial solitary waves when the upper fluid is bounded above (also called the rigid-lid approximation) and the lower fluid has finite depth. Evans & Ford (1996) and Laget & Dias (1997) have computed interfacial solitary waves for the full Euler equations. Turner & Vanden-Broeck (1988) followed the solitary waves numerically and found that they broaden at some critical values of the wave speed. The waves approach a limiting configuration where the fluid interface is of permanent form and connects two uniform flows of constant but different depths. The interface is also called a 'front' and the flows are said to be 'conjugate' (Benjamin 1966; Lamb 2000). Recently Camassa *et al.* (2006) have performed comparisons between numerical computations of the Euler equations and different model equations, obtained when various assumptions are made: Korteweg–de Vries equation, Benjamin–Ono equation (Benjamin 1967; Ono 1975) and the intermediate–long wave (ILW) equation (Joseph 1977).

When the effect of interfacial tension is considered, the upper fluid is bounded above and the lower fluid is infinitely deep, Benjamin (1992) derived a weakly nonlinear long-wave evolution equation that admits a new kind of solitary wave with decaying oscillations on the tail. In the same configuration, solitary waves have been computed for the full Euler equations by Calvo & Akylas (2003) in two dimensions and by Părău, Vanden-Broeck & Cooker (2007) in three dimensions (see also Kim & Akylas 2006). Gravity–capillary interfacial waves were also calculated by Laget & Dias (1997), where both fluids either have finite depth, or are of infinite depth. An analytical study of interfacial gravity–capillary waves between two infinite layers of perfect fluids, based on the central manifold reduction theorem and normal form theory, was considered by Dias & Iooss (1996).

There are far fewer results valid in the presence of the free surface. One reason for the small number of studies considering the effect of the free surface on interfacial waves is the difficult problem of treating computationally and analytically the nonlinear interactions between the external ('fast') and internal ('slow') modes of oscillation. This problem is absent when assuming the rigid-lid approximation. Recently Craig, Guyenne & Kalisch (2005) have derived Hamiltonian long-wave expansions for free surface and interfaces in two dimensions, and they found new phenomena compared with the rigid-lid approximation, even when only weakly nonlinear waves were studied. For example, in the rigid-lid case the interfacial solitary waves were found to change their sign only once when varying some parameters, from being waves of elevation to being waves of depression (see Benjamin 1966), while Craig *et al.* (2005) have found that this change of sign can happen twice when the free surface is present.

A small number of papers deal with nonlinear interfacial waves with free-surface boundary conditions, when only the effect of gravity is considered: Moni & King (1995) have computed solitary waves; Peters & Stoker (1960) and Kakutani & Yamasaki (1978) have derived coupled Korteweg–de Vries equations for long waves at the interface when the free-surface boundary conditions are considered, and then studied solitary waves for these equations; and Akylas & Grimshaw (1992), Michallet & Dias (1999) and Părău & Dias (2001) have computed generalized solitary waves, or solitary waves with non-decaying oscillatory tails. Analytical studies of generalized solitary waves in this configuration have been performed by Iooss, Lombardi & Sun (2002) and Lombardi & Iooss (2003). Dias & Il'ichev (2001) have studied the waves for a model equation. They have shown that 'slow' fronts connecting two conjugate states exist, but they have ripples in their tails. Generalized solitary waves and fronts have also been considered in coupled model equations by Fochesato, Dias & Grimshaw (2005). Rusås & Grue (2002) and Fructus & Grue (2004) have calculated solitary waves and fronts in the related problem of three-layer fluids. In this configuration Lamb (2000) has also computed conjugate flows. In the related problem of an intrusion layer in a stationary incompressible three-layer system, both periodic and solitary waves have been studied by Forbes, Hocking & Farrow (2006) and Forbes & Hocking (2006), respectively.

The surface and interfacial tension forces can have a strong influence on interfacial waves with a wavelength of centimetres and are especially important for the experimental studies of the interfacial solitary waves. There are very few numerical or analytical results when the surface or interfacial tension forces are included. Iooss (1999) has considered bifurcating periodic waves in different configurations. Barrandon & Iooss (2005) have proved that there are small-amplitude gravity–capillary solitary waves when there is strong surface tension, no interfacial tension and the bottom layer is infinite. At leading order these solutions satisfy the Benjamin–Ono equation. A new integral formulation of two fluids separated by an interface and bounded above by a free surface in the presence of surface and interfacial tension was recently derived by Haut & Ablowitz (2009). In a three-layer fluid configuration Grimshaw & Christodoulides (2008) have studied asymptotically the so-called gap-solitons that occur when there is a gap between two branches of the dispersion relation.

In this paper, we present computations of new solitary waves in two-layer fluids with a free surface, when the effect of surface or interfacial tension is considered. Comparisons with previous solutions computed for rigid-lid approximations are performed. Limiting configurations for these gravity–capillary solitary waves are considered, and in particular broadening is observed to occur.

The structure of this paper is as follows. The problem formulation together with a study of the dispersion relation is given in the next section. The numerical method is described in § 3, with the results being presented in § 4. Finally, in § 5 we discuss our results.

2. Formulation

The two-fluid system consists of a fluid with constant density ρ_1 lying below a lighter fluid that has constant density ρ_2 ($\rho_2 < \rho_1$), and is shown in figure 1. The 1 and 2 subscripts are used to label the fluids, i.e. fluid 1 is in the lower layer and fluid 2 is in the upper layer. We introduce Cartesian coordinates (x, y) so that the x-axis coincides with the unperturbed interface between the two fluids and the y-axis is vertical. The acceleration due to gravity, g, acts in the negative y-direction. We account

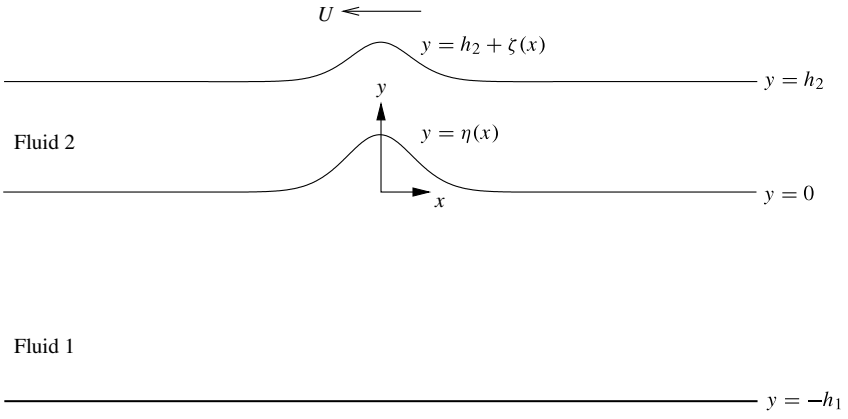

FIGURE 1. Physical domain of the two-fluid system.

for the effect of surface tension by including a constant surface tension, σ_F, on the free surface and a constant interfacial tension, σ_I, on the interface between the two layers. The lower layer is bounded below by a horizontal rigid bed at $y = -h_1$, while the upper layer is bounded above by a free surface. The unperturbed depths of the lower and upper layers are h_1 and h_2, respectively, where both h_1 and h_2 are positive. The undisturbed free surface is at $y = h_2$. We restrict our attention to steady flows and fix a frame of reference moving with the solitary waves, which translate in the negative x-direction at a constant speed U. The interfacial wave profile is given by $y = \eta(x)$ and the free-surface wave profile by $y = h_2 + \zeta(x)$, where we assume that $\eta(x)$ and $\zeta(x)$ together with their derivatives decay to zero as $|x| \to \infty$.

We assume that the fluids are inviscid and incompressible, and that the flow is irrotational in both layers. Therefore there exists a velocity potential, $\Phi_j(x, y)$, in fluid j $(j = 1, 2)$ such that

$$\boldsymbol{u}_j = (u_j, v_j) = \left(\frac{\partial \Phi_j}{\partial x}, \frac{\partial \Phi_j}{\partial y} \right), \tag{2.1}$$

which in conjunction with the incompressibility condition implies that each potential function satisfies Laplace's equation,

$$\nabla^2 \Phi_j = 0. \tag{2.2}$$

Far from the disturbance, the motion of the fluids becomes that of a uniform stream, so that

$$\boldsymbol{u}_j = \left(\frac{\partial \Phi_j}{\partial x}, \frac{\partial \Phi_j}{\partial y} \right) \to (U, 0) \quad \text{as } |x| \to \infty. \tag{2.3}$$

Higher derivatives of the velocity potentials with respect to x and y decay to zero as $|x| \to \infty$. To proceed, we non-dimensionalize by choosing h_2 and U as the length and velocity scales, respectively. The velocity decay condition becomes

$$\frac{\partial \Phi_j}{\partial x} \to 1 \quad \text{as } |x| \to \infty, \tag{2.4}$$

where all quantities are now understood to be dimensionless. The free-surface profile is given by $y = 1 + \zeta(x)$ and the bed lies at $y = -1/H$, where H is the depth ratio,

$$H = \frac{h_2}{h_1}. \tag{2.5}$$

The kinematic conditions involving the velocity potential, Φ_1, on the bed and the interface are

$$\frac{\partial \Phi_1}{\partial y} = 0 \quad \text{and} \quad \frac{\partial \Phi_1}{\partial x}\eta' = \frac{\partial \Phi_1}{\partial y}, \tag{2.6}$$

respectively. The kinematic conditions involving Φ_2 on the interface and the free surface are

$$\frac{\partial \Phi_2}{\partial x}\eta' = \frac{\partial \Phi_2}{\partial y} \quad \text{and} \quad \frac{\partial \Phi_2}{\partial x}\zeta' = \frac{\partial \Phi_2}{\partial y}, \tag{2.7}$$

respectively. The prime denotes differentiation with respect to x. Application of the Bernoulli equation to the free surface, $y = 1 + \zeta(x)$, yields the dynamic condition

$$\frac{1}{2}F^2(|\nabla \Phi_2|^2 - 1) + \zeta - \tau_F \frac{\zeta''}{[1 + (\zeta')^2]^{3/2}} + \epsilon_F p_D = 0, \tag{2.8}$$

where the Froude number, F, and the free-surface Bond number, τ_F, are defined by

$$F^2 = \frac{U^2}{gh_2} \quad \text{and} \quad \tau_F = \frac{\sigma_F}{\rho_2 g h_2^2}. \tag{2.9}$$

The $\epsilon_F p_D$ term represents a pressure forcing, which is a localized imposed deviation from the hydrostatic pressure. The pressure strength on the free surface is determined by the size of ϵ_F. The localized pressure forcing function, p_D, is defined later. The purpose of p_D is to facilitate the calculation of so-called 'forced' solitary waves, from which we are able to obtain pure solitary waves by reducing the strength of the forcing term to zero by the process of parameter continuation (e.g. Vanden-Broeck 2010). By applying the Bernoulli equation to both fluids at the interface, we obtain the dynamic condition

$$\frac{1}{2}F^2[|\nabla \Phi_1|^2 - R|\nabla \Phi_2|^2 - (1 - R)] + (1 - R)\eta - \tau_I \frac{\eta''}{[1 + (\eta')^2]^{3/2}} - R\epsilon_I p_D = 0, \tag{2.10}$$

where $R = \rho_2/\rho_1$ is the density ratio ($0 < R < 1$), $\tau_I = \sigma_I/(\rho_1 g h_2^2)$ is the interfacial Bond number, and ϵ_I is the strength of the interfacial pressure disturbance. The problem therefore reduces to finding η, ζ and Φ_j that satisfy the linear and nonlinear boundary conditions in (2.4), (2.6)–(2.8) and (2.10), and where the velocity potentials must also satisfy Laplace's equation in each layer.

2.1. *Dispersion relation*

To obtain the dispersion relation for the two-fluid system, we substitute a linear periodic wavefunction, with wavenumber k, into the governing equations and boundary conditions. After linearization and simplification, we obtain (see also Părău & Sasu 1996)

$$(F_{\pm}(k))^2 = \frac{b(k) \pm \sqrt{b^2(k) - 4a(k)c(k)}}{2ka(k)}, \tag{2.11}$$

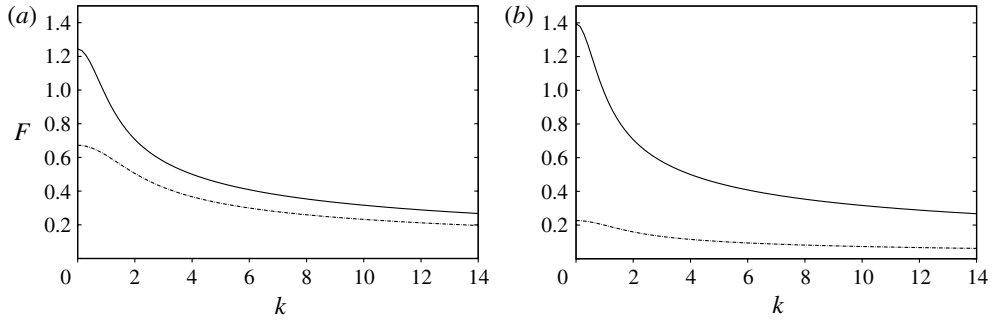

FIGURE 2. Dispersion relation curves for the gravity case, $\tau_F = \tau_I = 0$, with $H = 1$ and (*a*) $R = 0.3$ and (*b*) $R = 0.9$. In both (*a*) and (*b*) the 'fast' mode is shown as a solid line and the 'slow' mode as a dashed line.

where the positive root, $F_+(k)$, represents the 'fast' mode, and the negative root, $F_-(k)$, represents the 'slow' mode. The functions $a(k)$, $b(k)$ and $c(k)$ are

$$\left.\begin{aligned} a(k) &= 1 + R\tanh\left(\frac{k}{H}\right)\tanh(k), \\ b(k) &= \tanh\left(\frac{k}{H}\right) + \tanh(k) + k^2\left[\tau_I\tanh\left(\frac{k}{H}\right) + \tau_F\left(R\tanh\left(\frac{k}{H}\right) + \tanh(k)\right)\right], \\ c(k) &= (1 - R + \tau_I k^2)(1 + \tau_F k^2)\tanh\left(\frac{k}{H}\right)\tanh(k), \end{aligned}\right\} \tag{2.12}$$

and where R, H, τ_F and τ_I are constant parameters. In the long-wave limit, $k \to 0$, there are two critical values given by

$$(F_\pm^0)^2 = \frac{(1+H) \pm \sqrt{(1+H)^2 - 4H(1-R)}}{2H}, \tag{2.13}$$

where F_+^0 and F_-^0 $(< F_+^0)$ are the 'fast' and 'slow' critical Froude numbers, respectively, and the zero superscript indicates that $k = 0$. The values of $F_\pm^0$ depend on H and R but are independent of the Bond numbers.

When we set $\tau_F = \tau_I = 0$ in (2.11), it reduces to the dispersion relation for pure gravity waves (e.g. Michallet & Dias 1999). In this case both modes decrease monotonically as the wavenumber increases. Example dispersion relation curves for gravity waves are plotted in figure 2 for the parameters $H = 1$, $R \in \{0.3, 0.9\}$ and $\tau_F = \tau_I = 0$. We can see from the figure that, for a given value of the depth ratio, H, the separation between the modes grows larger as the density ratio, R, increases in value.

There are three combinations of Bond numbers that give rise to gravity–capillary waves: (i) $\tau_F \neq 0$ and $\tau_I = 0$; (ii) $\tau_F \neq 0$ and $\tau_I \neq 0$; and (iii) $\tau_F = 0$ and $\tau_I \neq 0$. In case (i), when only the surface tension is non-zero, the behaviour of the modes for large k is

$$F_+(k) \to +\infty \quad \text{and} \quad F_-(k) \to 0 \quad \text{as } k \to +\infty. \tag{2.14}$$

Therefore the slow mode behaves in a similar fashion to the pure gravity case for large k. However, when $k \ll 1$ the behaviour of both modes is governed by the size of the Bond number, τ_F. Expanding (2.11) in powers of k reveals the existence of two

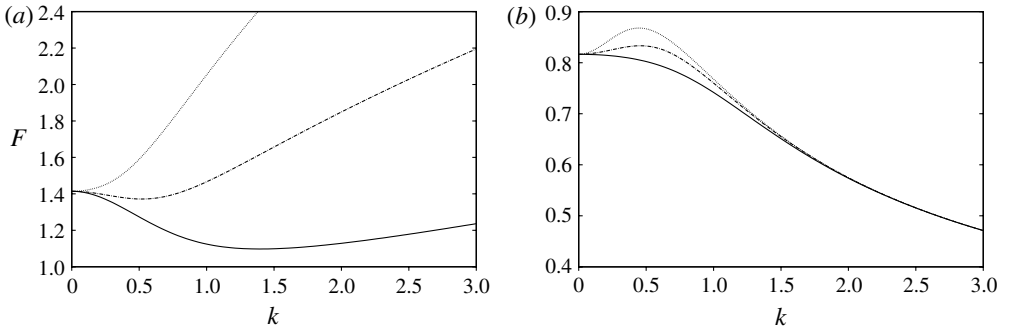

FIGURE 3. Dispersion relation curves for the gravity–capillary case, $\tau_F \neq 0$ and $\tau_I = 0$, with $H = 0.6$ and $R = 0.2$, showing (a) the 'fast' modes and (b) the 'slow' modes. In both (a) and (b), $\tau_F = 0.4$ (solid line), $\tau_F = 1.5$ (dashed line) and $\tau_F = 4$ (dotted line) are shown. Different F scales are used in the two figures to highlight the extrema.

critical Bond numbers, $\tau_F = \tau^*_{F_\pm}$. Details of the calculation are given in the Appendix and formulae for $\tau^*_{F_\pm}$ are given in (A 8). When $\tau_F < \tau^*_{F_+}$ the 'fast' mode decreases (as k increases) from its initial value to a local minimum. The 'slow' mode increases from its initial value to a local maximum when $\tau_F > \tau^*_{F_-}$. As k increases further, the 'fast' and 'slow' modes tend to infinity and zero, respectively, as stated in (2.14).

To demonstrate the behaviour of the modes for various values of the surface Bond number, τ_F, we plot the modes in figure 3 for the parameters $H = 0.6$, $R = 0.2$, $\tau_F \in \{0.4, 1.5, 4\}$ and $\tau_I = 0$. The 'fast' modes for the different values of the Bond number are shown in figure 3(a) and the 'slow' modes are shown in figure 3(b). For these parameters $F^0_+ \approx 1.414$, $F^0_- \approx 0.816$, $\tau^*_{F_+} \approx 2.556$ and $\tau^*_{F_-} \approx 0.630$, where the critical Froude numbers were calculated from (2.13) and the critical Bond numbers from (A 8). When $\tau_F = 0.4$ ($< \tau^*_{F_\pm}$), we can see from figure 3(a) that the 'fast' mode possesses a minimum for a positive value of k and the 'slow' mode decreases monotonically. At the highest value of the surface Bond number, $\tau_F = 4$ ($> \tau^*_{F_\pm}$), the 'fast' mode increases monotonically and the 'slow' mode possesses a non-zero maximum. When $\tau_F = 1.5$ the Bond number lies between the two critical Bond numbers, $\tau^*_{F_\pm}$, and both modes possess extrema at positive values of k. We can see from figure 3 that there is a spectral gap in (F, k)-space between the modes, e.g. $F = 1$ lies in the gap between the modes for all dispersion curves shown in the figure. However, the spectral gap is not present for all values of the parameters. As τ_F decreases, the spectral gap shrinks in size until the Froude number at the 'fast' mode's non-zero minimum will equal F^0_-, at which point the gap disappears. For example, when $\tau_F = 0.1$ there is no spectral gap. Since our aim is to find solitary waves, we are interested in those values of the Froude number that do not intersect the modes in (F, k)-space to avoid resonance with either mode. In summary, we are interested in parameters for which a spectral gap exists and Froude numbers that lie inside the gap.

The next case we consider is when both the surface and interfacial Bond numbers are non-zero. For large k the behaviour of the modes is

$$F_\pm(k) \to +\infty \quad \text{as } k \to +\infty. \tag{2.15}$$

Since the modes both tend to infinity as k becomes large, there cannot be a spectral gap between the modes. When searching for solitary waves we will therefore restrict our attention to values of the Froude number that fall below the 'slow' mode, so that

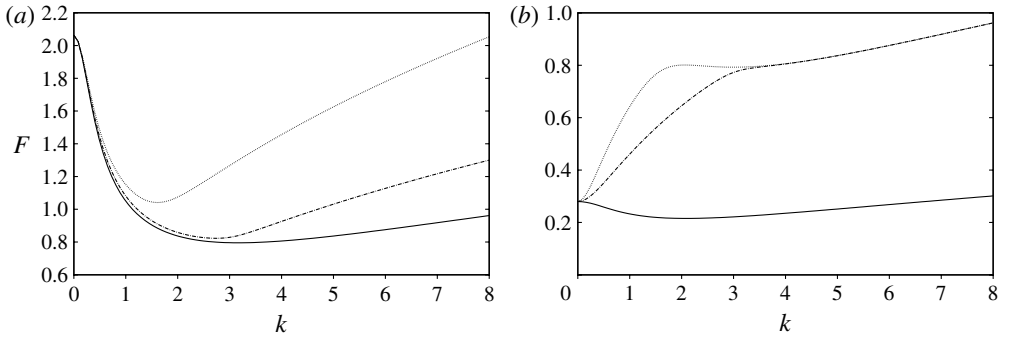

FIGURE 4. Dispersion relation curves for the gravity–capillary case, $\tau_F = 0.1$ and $\tau_I \neq 0$, with $H = 0.3$ and $R = 0.9$, showing (a) the 'fast' modes and (b) the 'slow' modes. In both (a) and (b), $\tau_I = 0.02$ (solid line), $\tau_I = 0.4$ (dashed line) and $\tau_I = 1$ (dotted line) are shown. Different F scales are used in the two figures to highlight the extrema.

we do not intersect the mode. Once again, an analysis of the dispersion relation for $k \ll 1$ reveals the presence of critical Bond numbers. Details are given in the Appendix and formulae are given in (A 9). We show the modes in figure 4 for $H = 0.3$, $R = 0.9$, $\tau_F = 0.1$ and $\tau_I \in \{0.02, 0.4, 1\}$. For these parameters the critical Froude numbers are $F_+^0 \approx 2.063$ and $F_-^0 \approx 0.280$. The 'fast' modes are shown in figure 4(a), where we can see that the different values of τ_I modify the mode but the behaviour is qualitatively similar, i.e. the mode decreases from the 'fast' critical value of the Froude number to a minimum before increasing as $k \to \infty$. Figure 4(b) shows the 'slow' modes for the same parameters. For $\tau_I \in \{0.4, 1\}$ the 'slow' mode increases as $k \to \infty$, but when $\tau_I = 0.02$ the mode possesses a minimum for positive k.

Although not considered here, the modes in the case when $\tau_F = 0$ and $\tau_I \neq 0$ display several interesting features (see Părău 2000 for more details). Firstly, provided H is large enough, the modes come together before separating, i.e. the 'fast' mode decreases to a minimum before increasing and the 'slow' mode increases to a maximum before decreasing. Therefore, for large wavenumbers, the behaviour of the modes is as if $\tau_F \neq 0$ and $\tau_I = 0$. Moreover, the gap between the modes can become very small, which severely limits the range of Froude numbers in which solitary waves may be found. For some parameters there is no gap between the modes.

3. Numerical method

The numerical scheme extends the one used by Laget & Dias (1997) for calculating interfacial waves in a channel of constant height by allowing the fixed top surface to become a free surface. The problem is solved numerically using a boundary integral equation technique based on Cauchy's integral formula. The complex potential,

$$w_j(z) = \Phi_j(x, y) + \mathrm{i}\Psi_j(x, y), \tag{3.1}$$

is introduced in each layer, where $\Psi_j(x, y)$ is the stream function in layer j. The physical plane, $z = x(w_j) + \mathrm{i}y(w_j)$, in each layer is mapped to $w_j(z)$ in the inverse plane. We choose $\Phi_1 = \Phi_2 = 0$ at $x = 0$ and define $\Phi_2 = g(\Phi_1)$, which provides the mapping between the velocity potentials. On the interface we set $\Psi_1 = \Psi_2 = 0$ so that $\Psi_1 = -\hat{H}$ $(= -1/H)$ on the bed, and $\Psi_2 = 1$ on the free surface. In terms of the potentials, the interface and free-surface profiles are $y(\Phi_1) = y(\Phi_1 + \mathrm{i}0)$ and $Y(\Phi_1) = y(\Phi_2 + \mathrm{i})$, respectively. Each layer is therefore mapped to an infinite strip of

constant height in the inverse plane. Application of the Cauchy integral formula to the lower layer, where the contour comprises the interface, its reflection in $\Psi_1 = -\hat{H}$ and lines joining them at infinity, gives

$$x'(\Phi_0) - 1 = \frac{1}{\pi}\left(\int_{-\infty}^{\infty} \frac{2\hat{H}(x'-1) - (\Phi_1 - \Phi_0)y'}{(\Phi_1 - \Phi_0)^2 + 4\hat{H}^2}\,\mathrm{d}\Phi_1 - \fint_{-\infty}^{\infty} \frac{y'}{\Phi_1 - \Phi_0}\,\mathrm{d}\Phi_1\right), \quad (3.2)$$

where the prime denotes differentiation with respect to Φ_1, the evaluation point, Φ_0, lies on the interface, and the second integral on the right-hand side is evaluated in the principal value sense. It is worth noting that for an infinitely deep lower layer the only change required to (3.2) is the omission of the first integral on the right-hand side. We can see this intuitively from the equation and the limit, $\hat{H} \to \infty$, or more formally by applying Cauchy's integral formula to a contour comprising the interface and an infinite semi-circle in the lower fluid.

In the upper fluid, we apply Cauchy's integral formula to a contour that follows the interface, the free surface and the lines that join them at infinity. By placing the evaluation point on the interface and then on the free surface, we are able to derive two integral equations. For Φ_0 on the interface we obtain

$$\frac{x'(\Phi_0)}{g'(\Phi_0)} - 1 = \frac{1}{\pi}\left(\int_{-\infty}^{\infty} \frac{(X'-g') - (g-g_0)Y'}{(g-g_0)^2 + 1}\,\mathrm{d}\Phi_1 - \fint_{-\infty}^{\infty} \frac{y'}{g-g_0}\,\mathrm{d}\Phi_1\right), \quad (3.3)$$

where $X(\Phi_1) = x(\Phi_2 + \mathrm{i})$ is the physical x-coordinate on the free surface and $g_0 = g(\Phi_0)$. When the evaluation point, $\Phi_{2,0} = g(\Phi_0)$, lies on the free surface we obtain

$$\frac{X'(\Phi_0)}{g'(\Phi_0)} - 1 = \frac{1}{\pi}\left(\int_{-\infty}^{\infty} \frac{(x'-g') + (g-g_0)y'}{(g-g_0)^2 + 1}\,\mathrm{d}\Phi_1 - \fint_{-\infty}^{\infty} \frac{Y'}{g-g_0}\,\mathrm{d}\Phi_1\right). \quad (3.4)$$

In the derivation of (3.3) and (3.4), references to Φ_2 have been eliminated in favour of Φ_1 and the mapping function, g. The free-surface Bernoulli equation (2.8) and the interfacial equation (2.10) become

$$\frac{1}{2}F^2\left(\frac{(g')^2}{(X')^2 + (Y')^2} - 1\right) + (Y-1) - \tau_F \frac{X'Y'' - X''Y'}{[(X')^2 + (Y')^2]^{3/2}} + \epsilon_F p_D = 0, \quad (3.5)$$

$$\frac{1}{2}F^2\left(\frac{1 - R\,(g')^2}{(x')^2 + (y')^2} - (1-R)\right) + (1-R)y - \tau_I \frac{x'y'' - x''y'}{[(x')^2 + (y')^2]^{3/2}} - R\epsilon_I p_D = 0, \quad (3.6)$$

respectively. We either set $\epsilon_F \neq 0$ or $\epsilon_I \neq 0$ to obtain forced waves. Although we could set the forcing strength to be non-zero on both interfaces in (3.5) and (3.6), we found it unnecessary in our calculations. When pure solitary waves are calculated, both pressure strengths will be zero. In the complex plane care must be exercised with the arguments of the pressure forcing function, p_D. On the interface and free surface the natural variables are Φ_1 and $g(\Phi_1)$, respectively. Therefore on the interface, we define

$$p_D(\Phi_1) = \exp\left(\frac{1}{\Phi_1^2 - 1}\right) \quad \text{for } |\Phi_1| < 1, \quad \text{and 0 elsewhere,} \quad (3.7)$$

and on the free surface we set

$$p_D(g) = \exp\left(\frac{1}{g^2 - 1}\right) \quad \text{for } |g| < 1, \quad \text{and 0 elsewhere.} \quad (3.8)$$

To reduce the integration range in (3.2)–(3.4) we exploit the symmetry of the solitary waves. The symmetry conditions are

$$\left.\begin{array}{llllllll} x(-\phi) = -x(\phi), & x'(-\phi) = x'(\phi), & y(-\phi) = y(\phi), & y'(-\phi) = -y'(\phi), \\ g(-\phi) = -g(\phi), & g'(-\phi) = g'(\phi), & & \\ X(-\phi) = -X(\phi), & X'(-\phi) = X'(\phi), & Y(-\phi) = Y(\phi), & Y'(-\phi) = -Y'(\phi), \end{array}\right\} \quad (3.9)$$

which reduce the integration range to $[0, \infty)$. From (3.9) we also have

$$y'(0) = 0, \quad Y'(0) = 0, \quad (3.10)$$

which enforces zero vertical gradients at the peaks of the solitary waves.

To solve the five equations (3.2)–(3.6), the interfacial potential, Φ_1, is discretized using N equally spaced points and the integrals are truncated and discretized. Since the velocity potential in the upper fluid has been eliminated from the equations, there is no requirement to discretize Φ_2. The five unknown values at each mesh point are x', y', g', X' and Y'. If we are given a set of values for y', then we find that the discretization of (3.2) may be written as the matrix equation,

$$\boldsymbol{A} \cdot \boldsymbol{p} = \boldsymbol{q}. \quad (3.11)$$

The $(N-1) \times (N-1)$ matrix $\boldsymbol{A}$ contains constant coefficients, $\boldsymbol{p}$ is a column vector comprising the values of $x'(\Phi_0) - 1$ at each mesh mid-point, and $\boldsymbol{q}$ is a column vector storing the values of the integrals over Φ_1, which depend on y'. Therefore, we compute $\boldsymbol{q}$ from the values of y' and solve (3.11) to obtain $\boldsymbol{p}$, and hence x' at each mesh mid-point. The values of x' at the mesh points are then obtained using five-point finite-difference formulae. Once the values of x' have been updated, (3.6) is used to update g' at the mesh points using the values of y' and the newly computed values of x'. The remaining unknowns are therefore y', X' and Y', and so the number has reduced from $5N$ to $3N$.

We employ Newton's iterative scheme to solve for the unknowns using a predefined tolerance to check for convergence. We will require $3N$ equations to complete the system and populate the Jacobian required by the method. We obtain $2(N-2)$ equations from evaluating (3.3) and (3.4) with Φ_0 at each mid-point (except the last one). The integrals are computed using the trapezoidal rule. Four more equations are provided by (3.10) and by ensuring that $y' = Y' = 0$ at the Nth point. The final N equations, which complete the system, come from the evaluation of (3.5) at each mesh point. We iterate until the residual error of the solution vector is less than a predefined value. At each stage the values of y, g and Y required in (3.3)–(3.6) are found by numerical integration of their respective derivatives, while the second derivatives required in (3.5) and (3.6) are calculated using five-point finite-difference formulae. The wave shape in the physical domain is then obtained by numerical integration of the solution. The wave shape for negative x is obtained from the wave's symmetry about $x = 0$.

To test the numerical accuracy of the method, we computed solutions for different mesh resolutions and truncated domain sizes. We varied the number of points between $N = 641$ and $N = 961$ to check that the solution was independent of the resolution. To verify that the domain truncation did not materially affect the solution, we preserved the mesh resolution and tested computational domains for which the length of the positive Φ_1 domain lay between 20 and 40. For each set of tested parameters, the residual error of the solution was always less than 10^{-10}. We found that the results were insensitive to the mesh parameters and so we chose $N = 641$ and $|\Phi_1| \leqslant 40$ for

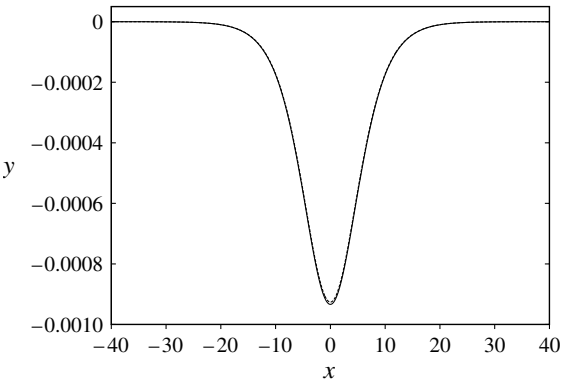

FIGURE 5. Comparison of interfacial solitary waves computed from (3.10) in Laget & Dias (1997) (solid line) and from our numerical model (dashed line). The model parameters are $H = 10$, $R = 0.1$, $\tau_F = \tau_I = 0.1$ and $F = 0.297$ ($< F^0_- \approx 0.298$). The computational domain has 641 points with $0 \leqslant \Phi_1 \leqslant 40$. The wave shape in the physical domain is obtained by numerical integration of the solution in the inverse plane and from the wave's symmetry.

most of our results. To further test the consistency and accuracy of our numerical method, we compared our numerical results with available analytical and numerical solutions. We compared our results for gravity waves with those of Moni & King (1995), with good agreement (see § 4.1). Small-amplitude capillary–gravity waves were compared with the analytical formula in § 3.4.1 of Laget & Dias (1997). They derived a Korteweg–de Vries equation for the interfacial wave between two layers of fluid subject to the rigid-lid approximation. To mimic the rigid lid we made the upper layer's depth much greater than that of the lower layer. Two example interfacial wave profiles are shown in figure 5, where the analytic formula has been appropriately scaled. The parameters used are $H = 10$, $R = 0.1$, $\tau_F = \tau_I = 0.1$ and $F = 0.297$ ($< F^0_- \approx 0.298$). From the figure we can see that the profiles are in good agreement. Comparisons were made with other values of the Froude number close to 0.297, again with good agreement.

To obtain solitary waves, a 'forced' solitary wave is computed for a value of the Froude number in the solitary wave range. The 'forced' wave is used as the initial guess in the next calculation, which has a slightly larger prescribed amplitude. At some point in the calculations the 'forced' wave changes from being a perturbation to the uniform stream to a perturbation of a pure solitary wave. Once this stage has been reached, the solitary wave is computed by setting the pressure strength to zero, thereby removing the pressure forcing, and the wave profile is recalculated. The purpose of the forced waves is to facilitate the computation of solitary waves.

4. Results

The values of the height ratio, H, density ratio, R, Froude number, F, and Bond numbers, τ_F and τ_I, are set and the wave profiles calculated using the numerical scheme described in the previous section.

4.1. *Solitary gravity waves*

In the first case we consider pure gravity waves, i.e. $\tau_F = \tau_I = 0$, and compare the results with Moni & King (1995), who computed in-phase solitary waves of elevation via conformal mapping techniques in the same two-fluid configuration. For

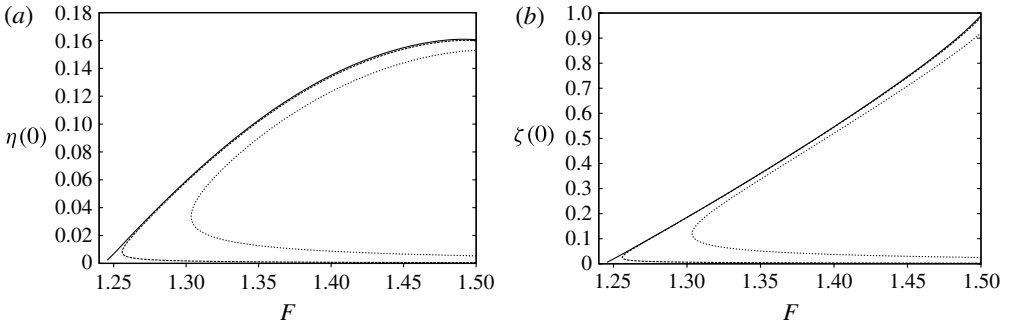

FIGURE 6. Relationship between the Froude number and (*a*) the interface amplitude, $\eta(0)$, and (*b*) the free-surface amplitude, $\zeta(0)$, for gravity waves with $H = 1$, $R = 0.3$ and $\tau_F = \tau_I = 0$. In both (*a*) and (*b*) the solid lines represent solitary waves while the dashed and dotted lines represent forced waves with $\epsilon_F = 0.01$ and $\epsilon_F = 0.1$, respectively. The 'fast' critical Froude number $F_+^0 \approx 1.244$.

the parameters $H = 1$ and $R = 0.3$, the upper critical Froude number, $F_+^0 \approx 1.244$. To obtain solitary waves we place the additional pressure on the free surface with $\epsilon_F = 0.1$ and set $F = 1.5$ initially. After computing the wave profile, we increase the free-surface amplitude, $\zeta(0)$, slightly and recalculate the profiles and the Froude number. Figure 6 shows how the wave amplitudes vary with Froude number. The results for the forced waves, indicated by dashed and dotted lines in the figure, show that the Froude number possesses a turning point. Lower values of ϵ_F move this point closer to the critical Froude number, $F_+^0 \approx 1.244$, and the whole curve closer to the solitary wave curve and Froude number axis. The turning point in the curve marks the region where the waves bifurcate from a uniform stream perturbation to a forced solitary wave. The pure solitary wave is then obtained by setting $\epsilon_F = 0$ and recomputing the wave profile. For $F = 1.404$, Moni & King (1995) computed the free-surface and interfacial amplitudes to be 0.552 and 0.134, respectively, whereas we found them to be 0.562 and 0.137. The difference is most likely to be due to the increased resolution used here. The wave profile shown in figure 7 is comparable to the wave in figure 2 of Moni & King (1995), for $F = 1.404$.

4.2. *Solitary gravity–capillary waves* ($\tau_F \neq 0, \tau_I = 0$)

Next we include the effects of surface tension by setting $\tau_F \neq 0$ while leaving $\tau_I = 0$. We focus our attention on a density ratio of $R = 0.9$, which is close to a realistic experimental value (e.g. Mercier *et al.* 2011). In the ocean the density ratio is approximately 0.99 or higher (e.g. Farmer & Dungan Smith 1980). The search for solitary waves is conducted for Froude numbers between the 'slow' critical value, F_-^0, and 'fast' critical value, F_+^0. Figure 8 shows the relationship between the Froude number and the wave amplitudes. A strong value of τ_F ($> \tau_{F_+}^*$) is chosen so that the 'fast' mode increases monotonically. We find solitary waves of depression on both surfaces for Froude numbers close to F_+^0. An almost linear relationship is found between the amplitudes of the waves on the free surface and the interface, with $\eta(0)$ remaining between 21 % and 24 % of $\zeta(0)$ for the range of Froude numbers shown in figure 8. The wave profiles for $F = 0.857$ are shown in figure 9(*a*) for $H = 3$, $R = 0.9$, $\tau_F = 0.6$ and $\tau_I = 0$. For these parameters, $\tau_{F_+}^* \approx 0.572$. To investigate the effect on the wave profiles of lowering the surface tension below the critical value, $\tau_{F_+}^*$, we gradually reduce τ_F and recompute the wave shapes. Using the profiles

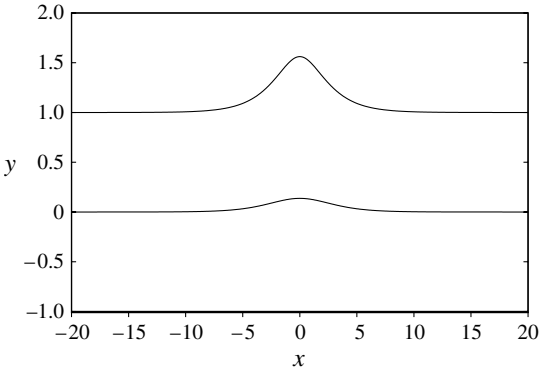

FIGURE 7. Gravity wave profiles on the interface and free surface for $H = 1$, $R = 0.3$ and $F = 1.404$. The bed is at $y = -1$. The interfacial and free-surface amplitudes are 0.137 and 0.562, respectively.

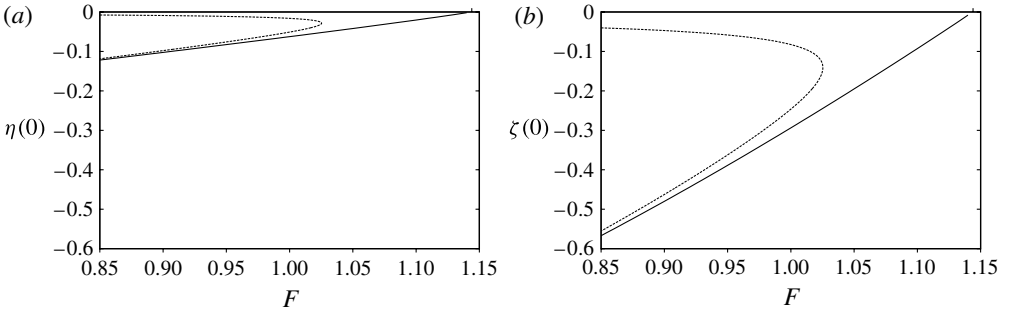

FIGURE 8. Relationship between the Froude number and (*a*) the interface amplitude, $\eta(0)$, and (*b*) the free-surface amplitude, $\zeta(0)$, for gravity–capillary wave calculations. In both (*a*) and (*b*) the solid and dashed lines represent solitary and forced waves, respectively. The parameters are $H = 3$, $R = 0.9$, $\tau_F = 0.6$, $\tau_I = 0$ and $\epsilon_F = 0.1$ for the forced waves. The 'fast' critical Froude number, $F^0_+ \approx 1.144$, is indicated by the top-right tick mark.

for $F = 0.857$ shown in figure 9(*a*), we gradually decrease τ_F so that the 'fast' mode of the dispersion relation develops a minimum, which approaches the prescribed value of F. Using a step size of 0.01 for τ_F we were able to decrease τ_F to 0.14 before $F = 0.857$ intersects the 'fast' mode, whereupon the calculations are terminated. The wave profiles are shown in figure 9(*b*), where the free-surface and interface profiles have been plotted on different vertical scales for clarity. The qualitative change in the wave profiles as τ_F decreases from 0.6 to 0.16 is that the waves now exhibit in-phase damped oscillations away from $x = 0$. The profiles resemble wavepackets in a manner consistent with solutions to the steady nonlinear Schrödinger equation (see § 4 in Laget & Dias 1997). The decrease in τ_F also reduces the wave amplitudes considerably, e.g. the free-surface amplitude has decreased in magnitude from -0.555 for $\tau_F = 0.6$ to -0.066 for $\tau_F = 0.14$. This is to be expected since the difference between the Froude number and the lower critical Froude number has decreased.

For Froude numbers close to, but greater than, the lower critical value, F^0_-, we expect solitary waves to bifurcate from a uniform flow (Barrandon & Iooss 2005). The presence of a wave of elevation or depression on the interface was shown to

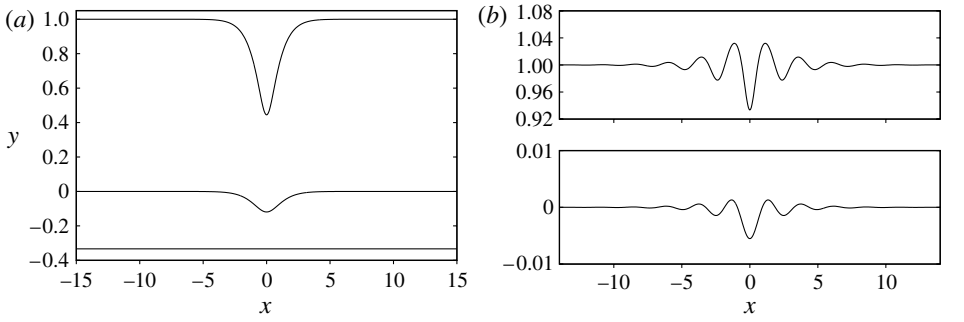

FIGURE 9. In-phase depression solitary waves for $H = 3$, $R = 0.9$, $\tau_I = 0$ and $F = 0.857$ for (a) strong surface tension, $\tau_F = 0.6$ ($> \tau^*_{F_+}$), and (b) weak surface tension, $\tau_F = 0.16$ ($< \tau^*_{F_+}$), where the profiles are shown separately using different scales on the y-axis.

depend on H by Laget & Dias (1997) for gravity waves in a rigid-lid approximation. In their calculations, when H is less than a critical value, $H^* = \sqrt{R}$, a wave of elevation is present on the interface. Conversely, when $H > H^*$ a depression wave was found on the interface. Michallet & Dias (1999) showed that these results were also true for generalized gravity solitary waves in the presence of a free surface, but H^* has a more complicated form (see also Kakutani & Yamasaki 1978). To obtain solitary waves from our calculations, we place the pressure forcing on the interface. We were unable to find solitary waves with the pressure forcing on the free surface. In our first simulation we set $H = 3$, $R = 0.9$, $\tau_F = 0.01$ and $\tau_I = 0$, and computed forced solitary waves with $\epsilon_I = -0.001$. The lower critical Froude number was $F^0_- \approx 0.160$. Figure 10(a) shows how the amplitudes of the forced and pure solitary waves vary with the Froude number. The wave amplitudes are of opposite sign, with a positive amplitude on the interface. The interface amplitude has a significantly greater magnitude than the amplitude of the free surface for a given value of the Froude number in this case. Different scales are used for the amplitudes to highlight the similarity between the curves. The solitary wave profiles computed for $F = 0.183$ are shown in figure 10(b), where the small depression on the free surface and the relatively large elevation on the interface can be seen. An interesting feature shown in figure 10(a) is the steepening of the solitary wave curve as the Froude number increases. When computing solitary waves in this region, we use small increments for the Froude number. The Froude number increment is 0.001 initially, and, when the calculation fails to converge, we decrease the increment by an order of magnitude and repeat the calculation. A fixed amplitude is attained by the solitary wave, and, as we increase the Froude number further, a plateau develops at the wave peak. Wave profiles are shown in figure 11 for three values of the Froude number, with the profile from figure 10(b) included for reference. The increasing accuracy in the Froude number that is required to calculate the broadening waves seems to indicate the presence of a limiting value of the Froude number, possibly for infinite broadening, which occurs for gravity waves in the rigid-lid configuration (Turner & Vanden-Broeck 1988). Our limiting value of F is close to F_{front} derived by Dias & Il'ichev (2001), where two conjugate flows are connected by fronts. To allow for the different scales used here and in Dias & Il'ichev (2001), we multiply our F by $\sqrt{H/(1+H)}$. After scaling $F = 0.183\,5857$ we obtain $F_{front} \approx 0.159$, which is in excellent agreement with (A.21) in Dias & Il'ichev (2001), which gives $F_{front} \approx 0.160$. In the absence of capillarity on

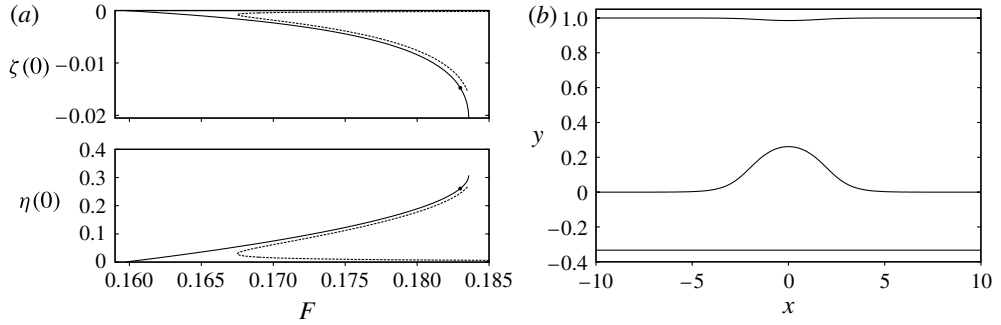

FIGURE 10. Results for $H = 3$, $R = 0.9$, $\tau_F = 0.01$ and $\tau_I = 0$ showing (a) the relationship between the Froude number, F, and the wave amplitudes, $\eta(0)$ and $\zeta(0)$, for forced waves with $\epsilon_I = -0.001$ (dashed lines) and pure solitary waves (solid lines), and (b) the solitary wave profiles corresponding to the solution for $F = 0.183$, which is marked by the dot on the solitary wave curve in (a).

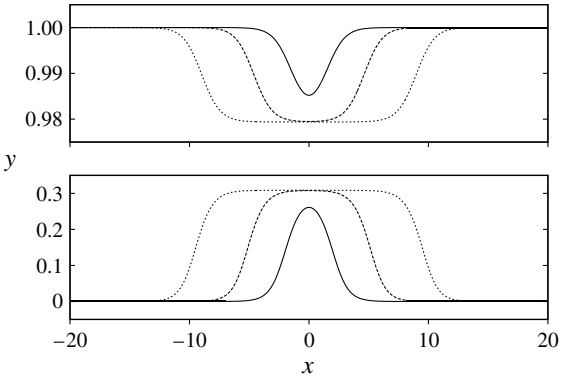

FIGURE 11. Broadening solitary waves for the parameters $H = 3$, $R = 0.9$, $\tau_F = 0.01$ and $\tau_I = 0$ with $F = 0.183$ (solid line), $F = 0.18358$ (dashed line) and $F = 0.1835857$ (dotted line). Different scales are used on the y-axis. The bed lies at $y = -1/3$.

the free surface, the same authors have shown that these fronts have ripples in their tails. However, when surface tension is present, we expect the ripples to disappear. We performed a further calculation with $R = 0.1$, $H = 3$ and $\tau_F = 0.05$. In this case we did not find broadening but instead find that the free-surface profile became increasingly sharp.

We now increase the relative depth of the lower fluid layer and examine the solitary waves for Froude numbers close to the critical value of the 'slow' mode. For $H = 0.3$, we set $R = 0.9$, $\tau_F = 0.5$ and $\tau_I = 0$ and put the pressure forcing on the interface with $\epsilon_I = 0.001$. The relationship between the wave amplitude and Froude number is similar to that shown in figure 10(a) but with a change of sign, i.e. a small wave of elevation on the free surface and a relatively large wave of depression on the interface. An example wave is shown in figure 12(a) for $F = 0.334$. We find that the solitary wave broadens as the Froude number increases past $F = 0.335$. Three wave profiles for different Froude numbers are shown in figure 12(b) to demonstrate the broadening. Once again, increasingly fine adjustments to the Froude number are required to obtain

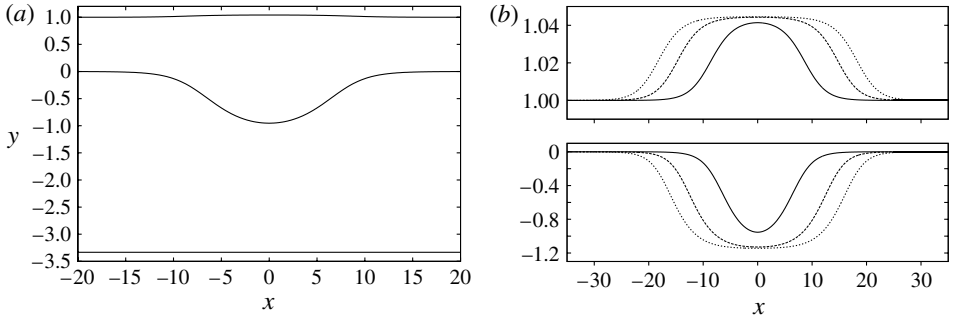

FIGURE 12. Solitary waves for $H = 0.3$, $R = 0.9$, $\tau_F = 0.5$ and $\tau_I = 0$ for (*a*) $F = 0.334$ and (*b*) $F = 0.334$ (solid line), $F = 0.335\,48$ (dashed line) and $F = 0.335\,4942$ (dotted line). In (*b*) the free-surface profiles are shown at the top, with the interface profiles below.

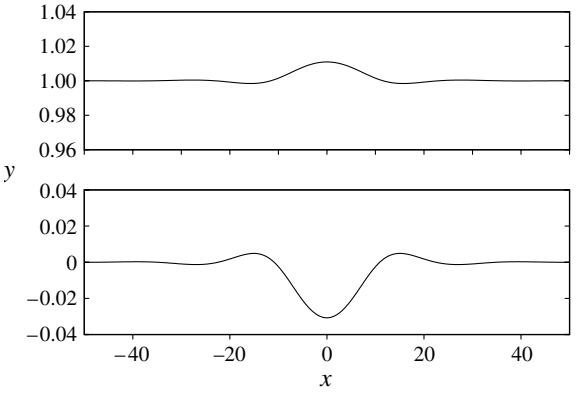

FIGURE 13. Wave shape for $H = 1$, $R = 0.5$, $\tau_F = 2.2$, $\tau_I = 0$ and $F = 0.5425$. The bed lies at $y = -1$.

solutions. The Froude number $F = 0.3355$ corresponds to $F_{front} \approx 0.161$ after the appropriate scaling, which is once again in excellent agreement with the results of Dias & Il'ichev (2001). The limiting amplitudes of the broadening interfacial wave shown in figures 11 and 12(*b*) are 0.309 and -1.143, respectively, or in terms of the total overall depth, they are 23 % and 26 %.

Finally we consider the case when $\tau_F > \tau_{F_-}^*$ so that a maximum appears in the 'slow' mode of the dispersion relation. Figure 13 shows the wave shapes for the parameters $H = 1$, $R = 0.5$, $\tau_F = 2.2$ and $\tau_I = 0$ for a Froude number, $F = 0.5425$. For these parameters, (A 8) gives $\tau_{F_-}^* \approx 1.569$. From the figure we see that the interfacial depression wave is out of phase with the free-surface elevation wave. Both waves have damped oscillations in their tails.

4.3. *Solitary gravity–capillary waves* ($\tau_F \neq 0$, $\tau_I \neq 0$)

Our final set of investigations are concerned with non-zero surface and interfacial tension. The two cases to consider are strong and weak interfacial tension, where the relative strength of the tension is determined with reference to the critical value of the interfacial tension, $\tau_{I_\pm}^*$, discussed at the end of § 2 and in the Appendix. For a sufficiently strong interfacial tension, the 'slow' mode increases from the 'slow'

critical Froude number, F_-^0. Solitary waves are calculated in the usual way, i.e. by computing forced solitary waves for a gradually increasing interfacial amplitude using a non-zero pressure forcing, ϵ_I, which is removed at a suitable juncture. In figure 14(*a*) we show an interfacial elevation wave that is out of phase with the free-surface depression wave. The parameters are $H = 0.3$, $R = 0.9$, $\tau_F = 0.1$, $\tau_I = 0.2$ and $F = 0.260$, which is below the critical value, $F_-^0 \approx 0.280$. The solitary waves were computed from forced waves with a negative value of ϵ_I. From the figure we can see that a wave of elevation lies on the interface, with a smaller wave of depression on the free surface. The wave orientation in this low-H configuration is the same as in the high-H case with $\tau_I = 0$, depicted in figure 10(*b*). When we reduce the value of τ_I so that the 'slow' mode develops a minimum, damped oscillations appear in the tails of the waves. The oscillations on the free surface are out of phase with respect to those on the interface. Example profiles are shown in figure 14(*b*) for $\tau_I = 0.06$. The reduction in amplitude for the low-τ_I waves is expected since the difference between the Froude number and the critical 'slow' Froude number has reduced ($F_-^* \approx 0.267$ for $\tau_I = 0.06$). For larger values of H, forced solitary waves are calculated using a positive value of ϵ_I. Pure solitary waves are calculated from these waves by reducing ϵ_I to zero. The wave profiles for $H = 3$ and $F = 0.11$ are shown in figure 15(*a*) for the parameters $H = 3$, $R = 0.9$, $\tau_F = 0.1$ and $\tau_I = 0.2$, for which the 'slow' critical Froude number, $F_-^0 \approx 0.160$. The elevation wave is now on the free surface, with the depression wave on the interface. Laget & Dias (1997) showed that solitary waves of opposite orientations could exist for the same parameters in the rigid-lid approximation. Specifically, they adjusted the relative depth of the fluid layers and followed the solitary waves for a given value of the Froude number (which they define with respect to the total depth). Since we now have a free surface, do solitary waves of opposite orientations continue to coexist? Using the wave profiles shown in figures 14(*a*) and 15(*a*), we perform parameter continuation on H and F separately. We take the wave profiles for the $H = 0.3$ case and increase the value of H and recompute the wave profiles, taking care to decrease the Froude number when it becomes too close to the critical Froude value, F_-^0 (which depends on H). We decrease H for the $H = 3$ case shown in figure 15(*a*) and recompute the profiles. We find that solitary waves coexist for a range of values of H and F. We show one pair of coexisting solitary waves in figure 15(*b*), where the parameters are $H = 1.5$, $R = 0.9$, $\tau_F = 0.1$, $\tau_I = 0.2$ and $F = 0.18$. The waves produced from the $H = 0.3$ and $H = 3$ cases are shown with solid lines and dashed lines, respectively. We conjecture that a region in the (F, H) plane exists in which solitary waves of opposite orientations coexist for identical parameters. The boundary of this region would be the free-surface generalization of (3.1) in Laget & Dias (1997) with non-zero surface tension taken into account.

5. Summary

In this paper we have presented numerical results obtained from the calculation of symmetrical solitary waves in a two-dimensional two-fluid system using the fully nonlinear equations. Gravity, surface tension and interfacial tension have been included in the formulation. Solitary waves are found by examining the dispersion relation with the aim of identifying the range of Froude numbers in which resonance with linear periodic waves cannot occur. We then seek solitary waves for Froude numbers in this range by a two-stage process. The first stage involves the computation of a forced wave, which is obtained by placing a localized pressure on one surface.

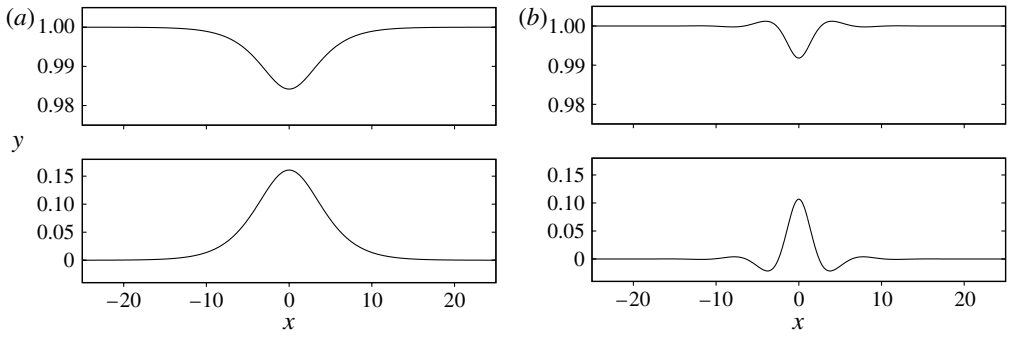

FIGURE 14. Solitary wave profiles for $F = 0.26$ with parameters $H = 0.3$, $R = 0.9$, $\tau_F = 0.1$ and (*a*) $\tau_I = 0.2$ and (*b*) $\tau_I = 0.06$. In (*a*) and (*b*) the free-surface profiles are shown at the top, with the interfacial profiles below. Different vertical scales are used for the free surface and the interface. The bed lies at $y = -10/3$.

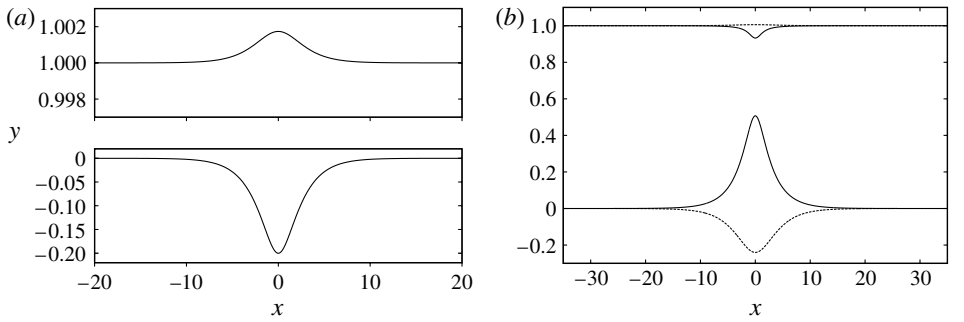

FIGURE 15. Wave profiles for $R = 0.9$, $\tau_F = 0.1$, $\tau_I = 0.2$ and (*a*) $H = 3$ with $F = 0.15$ and the bed at $y = -1/3$, and (*b*) $H = 1.5$ with $F = 0.18$ and the bed at $y = -2/3$. In (*a*) the free surface is shown at the top, with a different y-scale to the interfacial profile below. Panel (*b*) shows the coexistence of differently oriented solitary waves for identical parameters.

Parameter continuation is then used to increase the wave amplitude and recompute the wave profile. Repeating this calculation for progressively larger and larger amplitudes eventually leads to a wave that is a perturbation to a solitary wave rather than a disturbance to the free stream. In the second stage, the pressure forcing is simply removed to obtain the pure solitary wave. Once the solitary wave has been captured, parameter continuation may then be employed to examine the dependence of the waves on the parameters, e.g. the Froude number, the strength of the surface tension, etc.

When surface and interfacial tensions are omitted, we obtain gravity solitary waves that are in good agreement with previous results. The interfacial and free-surface waves are both of elevation. For non-zero surface tension there is a gap in the Froude number range in which solitary waves are found. Solitary waves of different orientations are found towards the upper and lower bounds of the Froude number range. Close to the upper bound, depression waves are found on both surfaces. When the surface tension is sufficiently strong, the 'fast' mode of the dispersion relation increases monotonically with increasing wavenumber and the solitary waves have sech^2-type profiles, similar to solutions of the Korteweg–de Vries equation. However,

when the surface tension is smaller than a critical value, the 'fast' mode develops a minimum at small values of the wavenumber. For Froude numbers close to the mode's minimum, the solitary waves develop in-phase damped oscillations in their tails. The overall profiles resemble wavepackets and are similar to solutions of the nonlinear Schrödinger equation. Solitary waves close to the lower bound of the Froude range change their orientation depending on the size of the depth ratio. When the upper layer is sufficiently thicker than the lower layer, the surfaces are drawn together at the crests of the waves. The wave orientations are reversed when the lower layer is significantly thicker than the upper layer, i.e. an elevation wave lies on the free surfaces with a depression wave on the interface. In both cases there are limiting values of the Froude number at which the wave amplitudes cease to increase and the waves broaden. For sufficiently high values of the surface tension, the 'slow' mode develops a maximum at small values of the wavenumber. Once again solitary waves computed for Froude numbers close to the extremum develop damped oscillations in their tails, although in this case they are out of phase.

Comparisons may be made between results obtained from our numerical model and the work of Mercier *et al.* (2011), which simulates the 'dead-water' phenomenon in two and three layers of water. In their two-layer experiments (see their figure 10) we see a depression solitary wave with an amplitude of around 3 cm beneath the boat, while the free surface is largely unperturbed. The undisturbed depths of the top and bottom layers in the experiments are 5 and 14 cm, respectively. In our numerical model, when surface tension is ignored, the dispersion relation indicates that short periodic waves will be present, but these are not observed in the experiment. However, when a realistic surface tension of 73 dyne m^{-1} is used, our numerical model predicts a depression solitary wave with an amplitude of approximately 3 cm (in the experimental units) for the parameters $H = 0.357$, $R = 0.976$, $\tau_F = 0.003$, $\tau_I = 0$ and a Froude number equal to 0.15. The Froude number is equivalent to a boat speed of 0.11 m s^{-1}, which is slower than the value 0.15 m s^{-1} quoted in Mercier *et al.* (2011). A better comparison could be made by capturing the reflected solitary waves after the boat had finished its journey, or by stopping the boat mid-journey and allowing the wave to continue to translate. However, isolation of these waves is difficult owing to the interactions of the transient waves generated in the experiment.

Finally, when both surfaces have non-zero tensions, the modes of the dispersion relation increase as the wavenumber becomes increasingly large. The range of Froude numbers for which solitary waves exist is bounded above by the minimum of the dispersion relation's 'slow' mode. The solitary waves are now out of phase. When the interfacial tension is lowered to a value for which the 'slow' mode decreases for small values of the wavenumber, damped oscillations appear in the tails of the waves. Out-of-phase solitary waves of both orientations are found to coexist for identical parameters.

Acknowledgements

This research has been supported by the EPSRC under grant EP/H008489/1. The authors would like to thank T. Dauxois for providing videos of some experimental results. The second author thanks the LMS for a Research in Pairs grant. Both authors would like to thank the anonymous referees for their valuable and constructive comments. The calculations presented in this paper were carried out on the High Performance Computing Cluster supported by the Research Computing Service at the University of East Anglia.

Appendix. Computation of the critical bond numbers

For long waves with wavenumber $k \ll 1$, the dispersion relation given in (2.11) may be expanded in powers of k^2 to get

$$F_{\pm}^2 = (F_{\pm}^0)^2 + \tfrac{1}{2}C_{\pm}(H, R, \tau_I, \tau_F)k^2 + O(k^4). \tag{A 1}$$

The sign of the $C_{\pm}$ term determines whether the Froude number increases or decreases as k increases from zero. If we denote the critical values of the interfacial and surface tensions by $\tau_{I_{\pm}}^*$ and $\tau_{F_{\pm}}^*$, respectively, then their values are obtained by satisfying $C_{\pm}(H, R, \tau_{I_{\pm}}^*, \tau_F) = 0$ or $C_{\pm}(H, R, \tau_I, \tau_{F_{\pm}}^*) = 0$. The coefficient $C_{\pm}$ can be expressed as

$$C_{\pm} = f_{1,\pm}(H, R) + \tau_I f_{2,\pm}(H, R) + \tau_F f_{3,\pm}(H, R), \tag{A 2}$$

where

$$f_{1,\pm}(H, R) = -\frac{1}{3H^3}\left(1 + H^3 \pm \frac{P}{Q} + 3HR(1 + H \pm Q)\right), \tag{A 3}$$

$$f_{2,\pm}(H, R) = \frac{1}{H}\left(1 \pm \frac{1 - H}{Q}\right), \tag{A 4}$$

$$f_{3,\pm}(H, R) = 1 + \frac{R}{H} \pm \frac{1}{Q}\left(-1 + \frac{R}{H} + H + 3R\right) \tag{A 5}$$

and

$$P(H, R) = (H - 1)(H^3 - 1) + 2HR(1 + H^2 + 3H(1 - R)), \tag{A 6}$$

$$Q(H, R) = \sqrt{(1 - H)^2 + 4HR}. \tag{A 7}$$

In the case of zero interfacial tension we find $\tau_{F_{\pm}}^*$ by setting (A 2) equal to zero and solving for $\tau_{F_{\pm}}^*$ to get

$$\tau_{F_+}^* = -\frac{f_{1,+}}{f_{3,+}} \quad \text{and} \quad \tau_{F_-}^* = -\frac{f_{1,-}}{f_{3,-}}. \tag{A 8}$$

When we take the limit of (A 8) with $H \to \infty$ we recover the well-known one-layer critical Bond number, $\tau_F^* = 1/3$. Figure 16(*a*) shows how the value of $\tau_{F_+}^*$ varies with R for $H \in \{0.9, 3\}$. When τ_F takes a value that is below the curve for a given R, the 'fast' mode will possess a minimum. Solitary waves computed for Froude numbers close to the minimum will have damped oscillations in their tails. In figure 16(*b*) the dependence of $\tau_{F_+}^*$ on H is plotted for $R \in \{0.1, 0.9\}$. Once again when τ_F takes a value below one of the curves for given values of H and R, the 'fast' mode will possess a minimum. As H increases, $\tau_{F_+}^*$ can be seen to tend towards $1/3$. However, when H decreases towards zero, the value of $\tau_{F_+}^*$ becomes singular. The curves shown in figure 16 imply that solitary waves in a two-layer system with a thin upper layer would need to have high surface tension in order to exceed the critical value, $\tau_{F_+}^*$.

An alternative solution to $C_{\pm} = 0$ is $\tau_{F_-}^* = -f_{1,-}/f_{3,-}$, which corresponds to a value of the surface tension at which the 'slow' mode develops a local maximum for small k. Figure 17 shows the critical value of $\tau_{F_-}^*$ for the same parameters as in figure 16. For given values of H and R the curves shown in figure 17 may be used to identify whether the surface tension exceeds the critical value, $\tau_{F_-}^*$. If $\tau_F > \tau_{F_-}^*$ then the 'slow' mode will possess a maximum at which we let $F_- = F_-^*$. Solitary waves for F close to, but greater than, F_-^* will have damped oscillations in their tails.

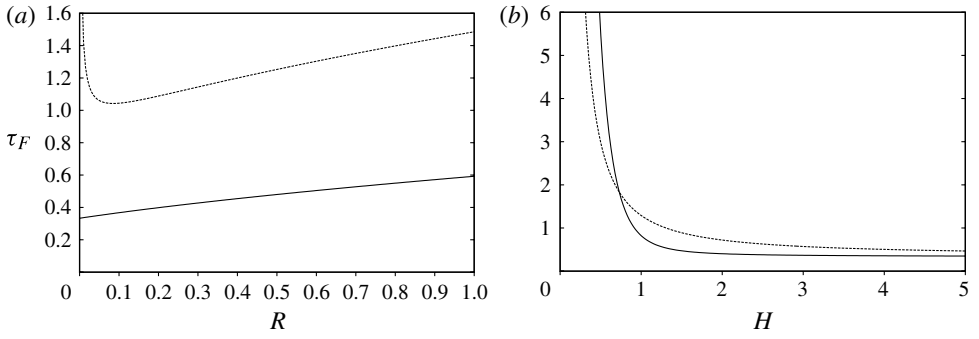

FIGURE 16. Curves showing the dependence of $\tau^*_{F_+}$ on (*a*) R and (*b*) H. In (*a*) the solid line is for $H = 3$ and the dashed line is for $H = 0.9$. In (*b*) the solid line is for $R = 0.1$ and the dashed line is for $R = 0.9$.

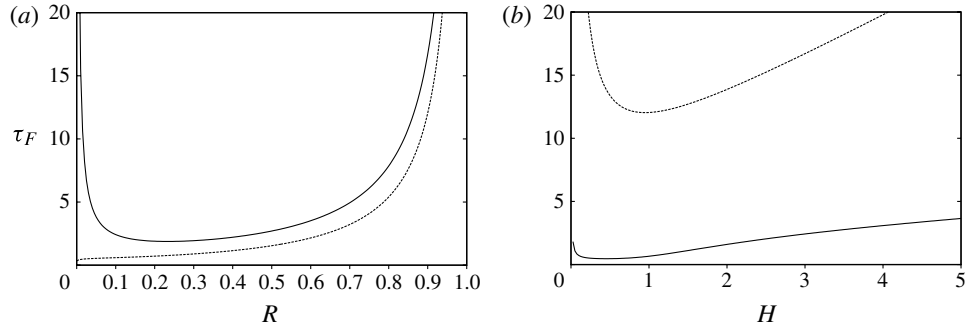

FIGURE 17. Curves showing the dependence of $\tau^*_{F_-}$ on (*a*) R and (*b*) H. In (*a*) the solid line is for $H = 3$ and the dashed line is for $H = 0.9$. In (*b*) the solid line is for $R = 0.1$ and the dashed line is for $R = 0.9$.

Equation (A 2) may also be used to find the critical values of the Bond numbers when both Bond numbers are non-zero. When either τ_F or τ_I is specified, we have

$$\tau^*_{F_\pm} = -\frac{\tau_I f_{2,\pm} + f_{1,+}}{f_{3,+}} \quad \text{or} \quad \tau^*_{I_\pm} = -\frac{\tau_F f_{3,\pm} + f_{1,+}}{f_{2,+}}, \tag{A 9}$$

respectively.

REFERENCES

AKYLAS, T. J. & GRIMSHAW, R. H. J. 1992 Solitary internal waves with oscillatory tails. *J. Fluid Mech.* **242**, 279–298.

BAINES, P. G. 1995 *Topographic Effects in Stratified Flows*. Cambridge University Press.

BARRANDON, M. & IOOSS, G. 2005 Water waves as a spatial dynamical system; infinite depth case. *Chaos* **15**, 037112.

BENJAMIN, T. B. 1966 Internal waves of finite amplitude and permanent form. *J. Fluid Mech.* **25**, 241–270.

BENJAMIN, T. B. 1967 Internal waves of permanent form in fluids of great depth. *J. Fluid Mech.* **29** (03), 559–592.

BENJAMIN, T. B. 1992 A new kind of solitary wave. *J. Fluid Mech.* **245**, 401–411.

CALVO, D. C. & AKYLAS, T. R. 2003 On interfacial gravity–capillary solitary waves of the Benjamin type and their stability. *Phys. Fluids* **15**, 1261–1270.

CAMASSA, R., CHOI, W., MICHALLET, H., RUSAS, P.-O. & SVEEN, J. D. 2006 On the realm of validity of strongly nonlinear asymptotic approximations for internal waves. *J. Fluid Mech.* **549**, 1–23.

CHOI, W. & CAMASSA, R. 1996 Weakly nonlinear internal waves in a two-fluid system. *J. Fluid Mech.* **313**, 83–103.

CHOI, W. & CAMASSA, R. 1999 Fully nonlinear internal waves in a two-fluid system. *J. Fluid Mech.* **396**, 1–36.

CRAIG, W., GUYENNE, P. & KALISCH, H. 2005 Hamiltonian long-wave expansions for free surfaces and interfaces. *Commun. Pure Appl. Maths* **58**, 1587–1641.

DIAS, F. & IL'ICHEV, A. 2001 Interfacial waves with free-surface boundary conditions: an approach via a model equation. *Physica* D **150** (3–4), 278–300.

DIAS, F. & IOOSS, G. 1996 Capillary–gravity interfacial waves in infinite depth. *Eur. J. Mech. (*B/*Fluids*) **15**, 367–393.

EKMAN, V. W. 1904 On dead water. *Norwegian North Polar Expedition, 1893-1896, Scientific Results* **5**, 1–150.

EVANS, W. A. B. & FORD, M. J. 1996 An integral equation approach to internal (2-layer) solitary waves. *Phys. Fluids* **8**, 2032–2047.

FARMER, D. M. & DUNGAN SMITH, J. 1980 Tidal interaction of stratified flow with a sill in Knight Inlet. *Deep-Sea Res.* A. *Oceanogr. Res. Papers* **27** (3–4), 239–246.

FOCHESATO, C., DIAS, F. & GRIMSHAW, R. 2005 Generalized solitary waves and fronts in coupled Korteweg–de Vries systems. *Physica* D **210**, 96–117.

FORBES, L. K. & HOCKING, G. C. 2006 An intrusion layer in stationary incompressible fluids. Part 2. A solitary wave. *Eur. J. Appl. Maths* **17** (05), 577–595.

FORBES, L. K., HOCKING, G. C. & FARROW, D. E. 2006 An intrusion layer in stationary incompressible fluids. Part 1. Periodic waves. *Eur. J. Appl. Maths* **17** (05), 557–575.

FRUCTUS, D. & GRUE, J. 2004 Fully nonlinear solitary waves in a layered stratified fluid. *J. Fluid Mech.* **505**, 323–347.

GRIMSHAW, R. & CHRISTODOULIDES, P. 2008 Gap-solitons in a three-layered stratified flow. *Wave Motion* **45** (6), 758–769.

HAUT, T. S. & ABLOWITZ, M. J. 2009 A reformulation and applications of interfacial fluids with a free surface. *J. Fluid Mech.* **631**, 375–396.

HELFRICH, K. R. & MELVILLE, W. K. 2006 Long nonlinear internal waves. *Annu. Rev. Fluid Mech.* **38**, 395–425.

IOOSS, G. 1999 Gravity and capillary–gravity periodic travelling waves for two superposed fluid layers, one being of infinite depth. *J. Math. Fluid Mech.* **1**, 24–61.

IOOSS, G., LOMBARDI, E. & SUN, S. M. 2002 Gravity travelling waves for two superposed fluid layers, one being of infinite depth: a new type of bifurcation. *Phil. Trans. R. Soc. Lond.* A **360**, 2245–2336.

JOSEPH, R. I. 1977 Solitary waves in a finite depth fluid. *J. Phys.* A **10**, L225–L227.

KAKUTANI, T. & YAMASAKI, N. 1978 Solitary waves on a two-layer fluid. *J. Phys. Soc. Japan* **45**, 674–679.

KIM, B. & AKYLAS, T. R. 2006 On gravity–capillary lumps. Part 2 Two-dimensional Benjamin equation. *J. Fluid Mech.* **557**, 237–256.

LAGET, O. & DIAS, F. 1997 Numerical computation of capillary–gravity interfacial solitary waves. *J. Fluid Mech.* **349**, 221–251.

LAMB, K. G. 2000 Conjugate flows for a three-layer fluid. *Phys. Fluids* **12**, 2169–2185.

LOMBARDI, E. & IOOSS, G. 2003 Gravity solitary waves with polynomial decay to exponentially small ripples at infinity. *Ann. Inst. Henri Poincaré* C. *Non-Linear Anal.* **20**, 669–704.

MERCIER, M. J., VASSEUR, R. & DAUXOIS, T. 2011 Resurrecting dead-water phenomenon. *Nonlin. Process. Geophys.* **18**, 193–208.

MICHALLET, H. & BARTHELEMY, E. 1998 Experimental study of interfacial solitary waves. *J. Fluid Mech.* **366**, 159–177.

MICHALLET, H. & DIAS, F. 1999 Numerical study of generalized interfacial solitary waves. *Phys. Fluids* **11**, 1502.

MONI, J. N. & KING, A. C. 1995 Guided and unguided interfacial solitary waves. *Q. J. Mech. Appl. Maths* **48** (1), 21.

ONO, H. 1975 Algebraic solitary waves in stratified fluids. *J. Phys. Soc. Japan* **39** (4), 1082–1091.

OSBORNE, A. R., BURCH, T. L. & SCARLET, R. I. 1978 The influence of internal waves on deep-water drilling. *J. Petrol. Tech.* **30** (10), 1497–1504.

PĂRĂU, E. 2000 Ondes interfaciales de flexion-gravité et de capillarité-gravité. PhD thesis, Univ. de Nice Sophia Antipolis, and West Univ. of Timisoara.

PĂRĂU, E. & DIAS, F. 2001 Interfacial periodic waves of permanent form with free-surface boundary conditions. *J. Fluid Mech.* **437**, 325–336.

PĂRĂU, E. & SASU, B. 1996 Surface–interface solitary waves. *Semin. Math. Anal. Appl.* **72**, 1–11.

PĂRĂU, E. I., VANDEN-BROECK, J.-M. & COOKER, M. J. 2007 Nonlinear three-dimensional interfacial flows with a free surface. *J. Fluid Mech.* **591**, 481–494.

PETERS, A. S. & STOKER, J. J. 1960 Solitary waves in liquid having non-constant density. *Commun. Pure Appl. Maths* **13**, 115–164.

PHILLIPS, O. M. 1966 *The Dynamics of the Upper Ocean*. Cambridge University Press.

RUSÅS, P.-O. & GRUE, J. 2002 Solitary waves and conjugate flows in a three-layer fluid. *Eur. J. Mech. (*B/*Fluids*) **21**, 185–206.

TURNER, R. E. L. & VANDEN-BROECK, J.-M. 1988 Broadening of interfacial solitary waves. *Phys. Fluids* **31**, 2486–2490.

VANDEN-BROECK, J.-M. 2010 *Gravity–Capillary Free-Surface Flows*. Cambridge University Press.